Advances in magneto-optical imaging applied to rock magnetism and paleomagnetism

Minoru Uehara, Cornelis Jacominus van Der Beek, Jérôme Gattacceca, Vladimir A. Skidanov, Yoann Quesnel

Geochemistry Geophysics Geosystems G3

Article
Volume 11, Number 5
12 May 2010
Q05Y09, doi:10.1029/2009GC002653
ISSN: 1525-2027

Published by AGU and the Geochemical Society

Advances in magneto-optical imaging applied to rock magnetism and paleomagnetism

Minoru Uehara
Department of Geophysics and Planetology, CEREGE, Aix-Marseille University, CNRS, F-13545 Aix-en-Provence, France (uehara@cerege.fr)

Cornelis Jacominus van der Beek
Laboratoire des Solides Irradiés, UMR 7642, Ecole Polytechnique, CNRS, IRAMIS, DSM, CEA, F-91128 Palaiseau CEDEX, France

Jérôme Gattacceca
Department of Geophysics and Planetology, CEREGE, Aix-Marseille University, CNRS, F-13545 Aix-en-Provence, France

Vladimir A. Skidanov
Institute for Design Problems in Microelectronics, Russian Academy of Sciences, Sovetskaja st. 3, Moscow 124681, Russia

Yoann Quesnel
Department of Geophysics and Planetology, CEREGE, Aix-Marseille University, CNRS, F-13545 Aix-en-Provence, France

[1] We present results of the magneto-optical imaging technique applied to rock samples. This technique measures the magnetic flux threading a magneto-optically active film, which rotates the polarization direction of transmitted light (Faraday rotation) and is directly placed on the sample. Through the analyzer of a reflected light microscope, the vertical component of the surface magnetic field of the sample is observed and can be quantified through a specific calibration procedure. Owing to the thin magneto-optically active film (5 μm) and the small sample-to-film distance (~1 μm), stray fields produced by magnetic grains in rocks carrying saturation isothermal remanent magnetization are successfully imaged with a spatial resolution of 10 μm. We can also image the surface field distribution of rocks carrying natural remanent magnetizations by modulating the analyzer angle. In addition to its high spatial resolution, this technique offers a direct comparison between magnetic and reflected light images. Therefore, this new technique appears to be a powerful tool to map and identify the carriers of magnetic remanence in rock samples.

Components: 5600 words, 7 figures.

Keywords: rock magnetism; paleomagnetism; magnetic microscopy; magneto-optical imaging; meteorite.

Index Terms: 1519 Geomagnetism and Paleomagnetism: Magnetic mineralogy and petrology; 1594 Geomagnetism and Paleomagnetism: Instruments and techniques.

Received 29 May 2009; **Revised** 8 January 2010; **Accepted** 2 February 2010; **Published** 12 May 2010.

Uehara, M., C. J. van der Beek, J. Gattacceca, V. A. Skidanov, and Y. Quesnel (2010), Advances in magneto-optical imaging applied to rock magnetism and paleomagnetism, *Geochem. Geophys. Geosyst.*, *11*, Q05Y09, doi:10.1029/2009GC002653.

Theme: Advances in Instrumentation for Paleomagnetism and Rock Magnetism
Guest Editors: M. Fuller, B. Goodman, J. Kirschvink, and K. Verosub

1. Introduction

[2] Magnetic microscopy is a powerful tool for the in situ identification and characterization of individual magnetic grains in rock samples. Recently, several scanning magnetic microscopes have been developed in particular to understand the magnetism of meteorites. Among these are Scanning Superconducting Quantum Interference Device (SQUID) microscopy [*Gattacceca et al.*, 2006; *Weiss et al.*, 2007], Scanning Giant Magneto-Resistance (GMR) microscopy [*Hankard et al.*, 2009], and Scanning Magneto-Impedance (MI) microscopy [*Uehara and Nakamura*, 2008].

[3] There are two fundamental problems specific to scanning magnetic microscopy. The first is related to the sensor dimension. For example, typical scanning SQUID sensors are several dozen micrometers in diameter, which limits spatial resolution to these scales. The second is the sample-to-sensor distance. Magnetic field lines emanating from magnetic grains fan out very rapidly as a function of distance from the sample surface, which leads to a concomitant reduction in spatial resolution of the probe. Furthermore, positioning errors may flaw the correlation of the magnetic image with other mineralogical observations, such as optical microscopy, scanning electron microscopy, and chemical analyses, and therefore hinder correct data interpretation.

[4] The magneto-optical imaging (MOI) technique, which utilizes the Faraday effect of magneto-optically (MO) active films, measures the magnetic flux threading a thin magnetic garnet film directly placed on the sample under study, with the main advantage that a full two-dimensional map is obtained by a single observation, without the need for scanning [*Bobyl et al.*, 2007; *Indenbom et al.*, 2002]. Since the distance between the garnet film and the sample is very small (1 μm in the present study), we can expect magnetic images with very high spatial resolution, limited only by the wavelength of visible light and the indicator film thickness. Moreover, any positioning error is, in principle, avoided. These merits suggest that the MOI technique can be very helpful to identify minerals carrying a magnetic moment in geological samples. The technique is, in fact, already widely used in material science for the observation of magnetic domain structures in magnetic materials [*Polyanski et al.*, 1999; *Welp et al.*, 2003] or flux penetration in superconductors [*Dorosinskii et al.*, 1992; *Jooss et al.*, 2002]. This technique has also been recently applied to geological samples [*Bobyl et al.*, 2007]. While the field sensitivity of the MOI films is orders of magnitude lower than that obtained for instance in scanning SQUID microscopy (with ~100 μm spatial resolution) [*Bending et al.*, 2004], and its spatial resolution is orders of magnitude less than that provided by, for example, Magnetic Force Microscopy (with μT field sensitivity), it does provide a very rapid two-dimensional mapping of magnetic properties with intermediate resolution and sensitivity that is more than sufficient for a wide variety of applications. In particular, the surface fields due to ferromagnetic grains in meteorites and terrestrial rocks are in the mT range and can be easily observed. *Bobyl et al.* [2007] conducted MOI observations on magnetite grains and magnetite-magnetite grain boundary regions in thin sections of skarns and serpentinites, carrying an isothermal remanent magnetization following application of a ±160 mT field perpendicular to the sample plane.

[5] Another magneto-optical effect known as the Kerr effect is also used in magnetic microscopy to characterize magnetic domain structures [*Hoffmann et al.*, 1990]. Since Kerr effect microscopy measures a rotation of the polarization when light is reflected from the surface of a magnetized material, it can only measure the magnetic field above a highly polished surface with high reflectance. On the other hand, MOI does not need a perfect polishing of the sample. Because MOI measures the magnetic flux passing through the indicator film, it can observe stray magnetic field even outside the magnetic material. Thus, the MOI technique has an advantage in the mapping of surface magnetic field distributions, although the thickness of the garnet film will result in some spatial resolution to be sacrificed as compared to Kerr effect microscopy.

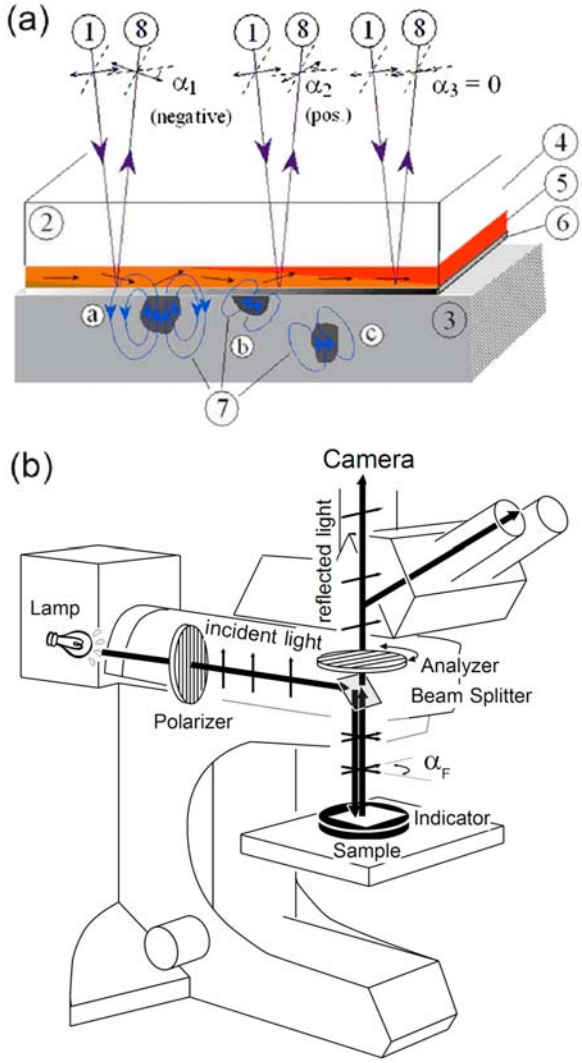

Figure 1. (a) Schematic representation of the magneto-optical imaging technique. Linearly polarized light is incident (indicated by 1) on the magneto-optical indicator (indicated by 2), which is simply placed on the rock sample (indicated by 3). It traverses the gadolinium-gallium-garnet substrate (indicated by 4) and the magneto-optically active film (indicated by 5) and is reflected on an Al mirror evaporated on the film surface (indicated by 6). The presence of magnetized grains (indicated by circled letters a, b, and c) in the rock sample (indicated by 3) results in nonzero local magnetic fields threading the magneto-optically active film (indicated by the field lines (indicated by 7)). As a consequence, the magnetization of the MO active layer, indicated by the near-horizontal arrows in the layer, undergoes a local out-of-plane rotation. The out-of-plane rotation causes a nonzero Faraday rotation α of the polarization direction of the light, which can be measured by passing the reflected light (indicated by 8) through the analyzer of a polarized light microscope. (b) Scheme of the magneto-optical imaging system using reflected light microscope.

[6] In this paper, we review the principle of the MOI technique and its specific development for the study of rock magnetism. A modulation technique, which increases the MOI sensitivity and allows for the measurement of the stray field from the natural remanent magnetization of geological samples, is also described. The observation of surface field distribution of rocks carrying natural remanent magnetizations is a significant improvement over the previous study [*Bobyl et al.*, 2007]. We show representative results on chondrite meteorites.

2. Magneto-Optical Imaging

[7] The MOI technique is based on the Faraday effect of a MO active magnetic layer (Figures 1a and 1b). We have used cubic Bi-doped rare earth iron garnet films, with a ferrimagnetic magnetization resulting from the sum of the moments of the Fe ions, situated on three differently coordinated crystalline sites. The films are grown by liquid phase epitaxy on paramagnetic doped gadolinium-gallium-garnet ($Gd_3Ga_5O_{12}$) substrates. The rare earth composition of the iron garnet films, similar to that used by *Dorosinskii et al.* [1992] and *Indenbom et al.* [2002], is chosen such that the easy axis of magnetization coincides with the film plane. Bi doping is performed to increase the saturation magnetization M_s, the corresponding Faraday rotation, and, ultimately, the film sensitivity. Figure 1 illustrates the principle of the imaging technique. Linearly polarized light is incident on the substrate (thickness 0.5 mm) and the garnet film (of thickness d = 5 μm), which is placed on the polished sample under study. The light is reflected on an Al layer of thickness 100 nm, evaporated on the garnet surface, and therefore traverses the MO active layer twice. This configuration of the garnet film is the same as that used in the previous study of *Bobyl et al.* [2007]. The presence of a nonzero magnetic induction, for example, due to the presence of magnetized grains in the rock sample, results in a rotation of the magnetization of the garnet, out of the film plane. While the in-plane component of the film's magnetization does not rotate the polarization angle of the light [*Polyanskii et al.*, 2004], the component of the magnetization parallel to the propagation direction of the light results in a Faraday rotation

$$\alpha_F = 2\,d\,V\,M_s \arctan\left[B_\perp/\left(B_\parallel + B_k\right)\right] \qquad (1)$$

of the polarization direction. The Faraday angle of rotation α_F is proportional to the Verdet constant of

the MO material (V) and its thickness d, and depends on the magnetic field components perpendicular ($B_\perp$) and parallel to the film ($B_\parallel$) [*Polyanskii et al.*, 2004]. B_k is the anisotropy field of the MO film. The observation of the reflected light image through an analyzing polarizer, oriented at an angle of $90° - \theta$ with respect to the incident polarization direction ($\theta \ll 90°$, nearly perpendicular configuration), allows for the direct visualization of the spatial distribution of the Faraday rotation angle. If the in-plane component of the applied field is small with respect to B_k, this corresponds to an image of the perpendicular component of the surface magnetic field, $B_\perp$.

[8] The intensity of the reflected light (I_{MOI}) is given by

$$I_{MOI} = I_0 T_\parallel \sin^2(\alpha_F + \theta) + I_0 T_\perp \cos^2(\alpha_F + \theta) \qquad (2)$$

where I_0 is the incident light intensity, $T_\parallel$ and $T_\perp$ are the transmission factors in the direction of parallel and perpendicular to the polarization plane of the analyzer, respectively, and $T_\perp/T_\parallel$ is the extinction ratio [*Flament et al.*, 2004]. A first-order expansion of equation (1) in α_F yields

$$I_{MOI} \approx \alpha_F I_0 (T_\parallel - T_\perp) \sin 2\theta + I_0 (T_\parallel \sin^2\theta + T_\perp \cos^2\theta); \qquad (3)$$

only the first term contains information about the magnetic field intensity. A development in θ,

$$I_{MOI} \approx 2\,\alpha_F\,\theta\, I_0 (T_\parallel - T_\perp) + I_0 T_\perp, \qquad (4)$$

shows that the uncrossing angle of polarizer and analyzer acts as an amplification factor. However, too large angles of θ increase the nonmagnetic contribution ($I_0\ T_\parallel \sin^2\theta + I_0\ T_\perp \cos^2\theta$), resulting in low image contrast. Thus, there is an optimum orientation angle of the analyzer that maximizes the contrast [*Flament et al.*, 2004]. This optimum angle (θ_{opt}), which depends on the field strength, is around $3 \sim 5°$ in the present study. Finally, the proportionality of the parasitic intensity $I_0\ T_\perp$ to $T_\perp$ shows that the use of efficient polarizers with $T_\perp \ll T_\parallel$ is essential.

[9] The proportionality of the image intensity to both the sign of the uncrossing angle θ and that of the Faraday rotation angle, and therefore to the perpendicular component of the magnetic field means that a contrast between positive and negative field components is observable. Thus, bright regions indicate nominally positive values of the perpendicular field component in an image with nominally positive θ ("positive image," $I_{MOI_{(+)}}$), while the corresponding image with nominally negative θ enhances negative values of the field component ("negative image," $I_{MOI_{(-)}}$). We normally use the "positive image" to observe the magnetic flux distribution emanating from strongly magnetized grains such as SIRM (saturation isothermal remanent magnetization). The resulting images are referred to as "direct" images.

[10] For the observation of weakly magnetized samples, such as natural remanent magnetization (NRM), we use a modulation technique that switches the analyzer angle between $\theta \pm \Delta\theta$ [*Indenbom et al.*, 2002]. This technique subtracts the positive and the negative images and measures only the magnetic contribution

$$\Delta I_{MOI} = I_{MOI(+)} - I_{MOI(-)} \approx 2\,\alpha_F\,\Delta\theta\, I_0\, T_\parallel. \qquad (5)$$

Furthermore, very weak magnetizations can be measured by enhancing the signal-to-noise ratio through simple averaging of multiple differential images (ΔI_{MOI}). The previous study by *Bobyl et al.* [2007] used another modulation technique to increase the sensitivity, in which the image of a sample with isothermal remanent magnetization (IRM) induced by a negative perpendicular magnetic field $H_\perp = -160$ mT is subtracted from the image acquired after the application of $H_\perp = +160$ mT. The change of the external applied field (±160 mT) implies that only the IRM can be measured, whereas our optical modulation method is fully nondestructive and allows one to measure NRM.

[11] Figure 1b schematically shows the present MOI system based on a reflected light optical microscope. The image acquisition and modulation sequence are controlled by a LabView-based PC system. A 12 bit color CCD camera (CFW-1312C Scion Corporation) or a 12 bit black and white CCD camera (Hamamatsu Photonics 4748 Orca II) is used for image acquisition. The present layout enables us to observe surface magnetic fields of opaque samples, such as rock samples, by placing the mirrored indicator on the surface (Figure 1a). The field sensitivity and the maximum attainable field with typical MO indicators are of the order of 0.1 mT and 200 mT, respectively; The latter corresponds to the saturation field of the garnet magnetization. These numbers are general bounds and

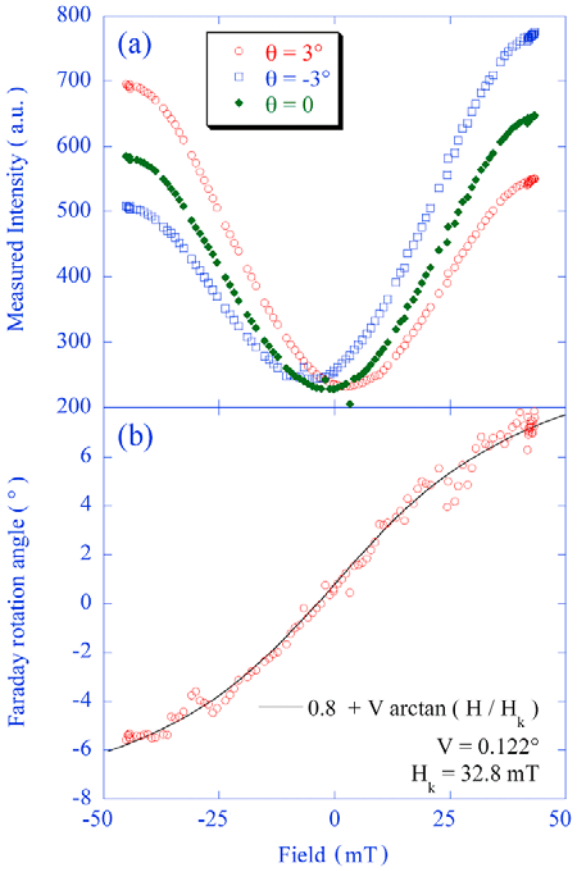

Figure 2. (a) Light intensity for three relative positions of the polarizer-analyzer pair, measured with respect to the fully crossed position. The deviation from a parabolic behavior at high fields is due to the saturation of the out-of-plane magnetization of the garnet film. (b) Absolute Faraday rotation angle as function of magnetic field for the garnet indicator used in Figures 3–7.

vary with garnet composition. A small negative (in-plane) magnetic anisotropy of the garnet implies a large field sensitivity of the order of 0.1 mT without image treatment, but a small saturation field. Oppositely, a large anisotropy is detrimental to the sensitivity but allows one to a have saturation fields of up to 200 mT. Boxcar integration of images (stacking) yields sensitivities down to 0.01 mT, while in general, a spatial resolution of 1–5 μm can be attained [*Indenbom et al.*, 2002]. To reduce noise or parasitic elements in the captured MO images (e.g., dust on the indicator surface, or the magnetic domain structure of the indicator itself), we took the mean of three images acquired with different spatial positions of the indicator with respect to the sample. Because the magnetic pattern is independent of the indicator's position, any image element that moves together with the indicator can be cancelled out by such a numerical noise reduction technique.

3. Results and Discussions

[12] Figure 2 demonstrates the characteristics of the garnet indicator used in the present observations, measured under vertically upward applied field. Figure 2a shows the light intensity (I_{MOI}) at the fully crossed position (θ = 0°), and around the optimum angle (θ = ±3°). For θ = 0°, we can only measure the absolute field strength by the I_{MOI} due to its symmetric feature with the field polarity. The curves are measured up to magnetic saturation, at which the field dependence of the Faraday rotation angle vanishes. Thus the measurable field range is controlled by the physical properties of the garnet indicator; at large perpendicular inductions, the resulting image is qualitative and nonlinear in the surface field intensity. On the other hand, the difference in intensity ΔI_{MOI} (between images taken for opposite angles ±θ) is a bijective function of the induction. Thus, the differential image is much more suitable for quantitative measurements. The absolute Faraday rotation angle as function of magnetic field (Figure 2b), which represents equation (1), shows that the product (2 d V M_s) is equal to 0.122°. Since M_s of this material is ~3 × 10^4 Am^{-2} and the thickness is 5 μm, the Verdet constant of this indicator is about 1 × 10^{-2} rad m A^{-1}. The anisotropy field value (H_k in Figure 2b) is 32.8 mT, this can be regarded as the maximum field strength up to which the Faraday rotation is linear in the perpendicular component of the induction. Although the characteristics of the MOI system vary between measurements because of variations of the temperature, of the intensity of the incident light, and so forth, it is possible to precisely estimate the field strength from MOI images by making a calibration curve for each measurement.

[13] Figure 3 shows a result of an MOI observation of a 6 mm thick polished section of the Agen (H5) ordinary chondrite meteorite. The sample was magnetically saturated by a 3 T vertically upward (out-of-plane) field and demagnetized by a 10 mT alternating field using the inline AF demagnetization of a 2G SQUID magnetometer. Because some meteorites contain ultrasoft magnetization components due to the presence of low-coercivity kamacite grains, we have demagnetized the sample to enhance the contrast of the signal produced by the carrier of the stable magnetization component (presumably

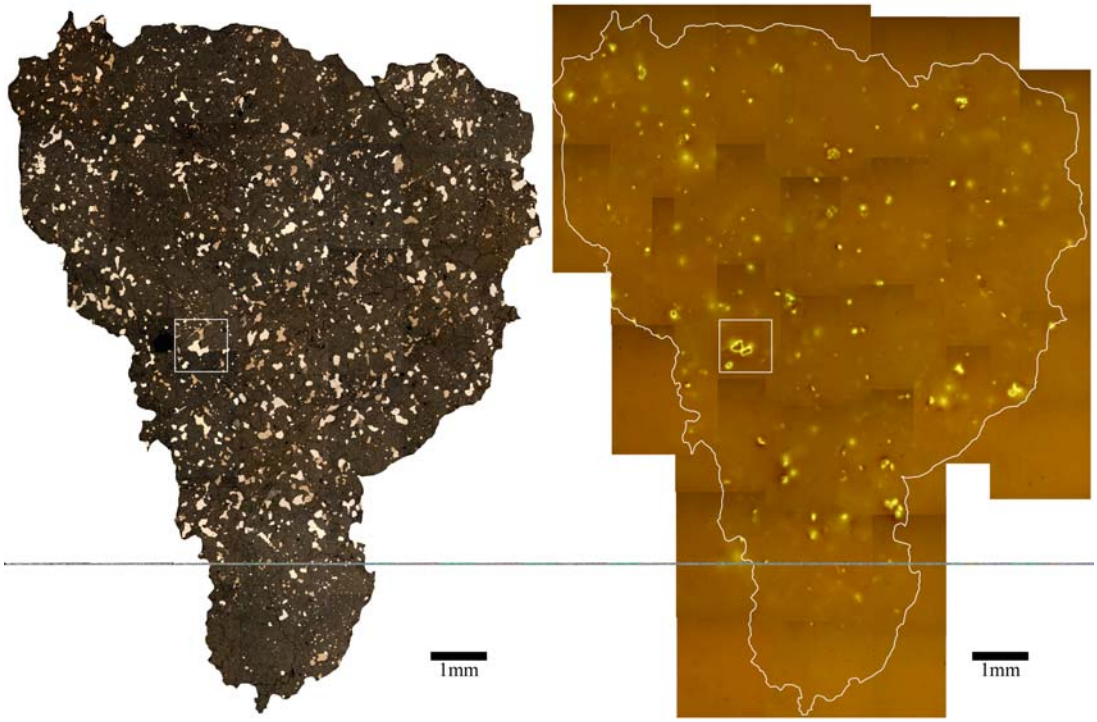

Figure 3. (left) Reflected light image and (right) direct MO image of a polished thick section of Agen (H5) ordinary chondrite carrying an upward pointing (out-of-page) SIRM. Brighter (darker) region corresponds to vertically upward (downward) surface magnetic field. The white box emphasizes an example of rimmed feature (see section 3 and Figure 5b).

tetrataenite). The Fe-Ni metal grains, which are the dominant magnetic minerals in ordinary chondrites, show up as bright spots in the MO image, indicating the presence of upward (out-of-plane) surface fields. Features with sharp contours correspond to the surface grains observed in reflected light. Features with fuzzy contours do not correspond to visible grains and originate from grains that are hidden under the surface of this 6 mm thick sample.

[14] Most MO patterns are bright solid spots, but several large grains show distinctive rimmed MO patterns (e.g., white box in Figure 3). There are two possible hypotheses explaining the rim pattern. The first is a shape effect. Above an uniformly magnetized infinite plane, the external field is always zero due to the mutual cancellation of individual source elements, but will result in a rimmed MO pattern for grains of finite width (e.g., MOI of magnetized ~200 nm thick and 1 mm^2 films in the work by *Jooss et al.* [2002]). This holds if the plane dimensions are at least ~30 times larger than the distance at which the field is measured. For MO observation of a 30 μm thin section, this would be the case for homogeneously magnetized grains that are at least ~500 μm in dimension. The second possibility is that the magnetization of the rim is larger than that of the bulk of the grain. These hypotheses can be checked by looking at the continuity of the rim: a continuous rim may correspond to a geometric effect, whereas a discontinuous rim must correspond to a discontinuous magnetized rim. Figure 4 shows enlarged images of grains in the Ausson (L5) ordinary chondrite meteorite, with discontinuous rim patterns showing up either as a large rim defect or as a broken line feature. These discontinuities probably correspond to the distribution of ferromagnetic minerals with higher magnetization at the rims of the grains. In fact, metallographic studies report that most metamorphic (type 4–6) ordinary chondrites contain zoned Fe-Ni grains, which have a central region with low-Ni content (about 30 ~ 40 wt % Ni, paramagnetic taenite) and an outer region with high Ni content [*Reisener and Goldstein*, 2003]. Since the Ni-rich region contains tetrataenite (ordered $Fe_{50}Ni_{50}$) with high coercivity [*Nagata and Funaki*, 1982; *Nagata et al.*, 1986; *Gattacceca et al.*, 2003], the rim MOI pattern may have some relationships with this tetrataenite rim. A third possibility is that the grain has a magnetization with radial symmetry. In that case the presence of a strong in-plane field

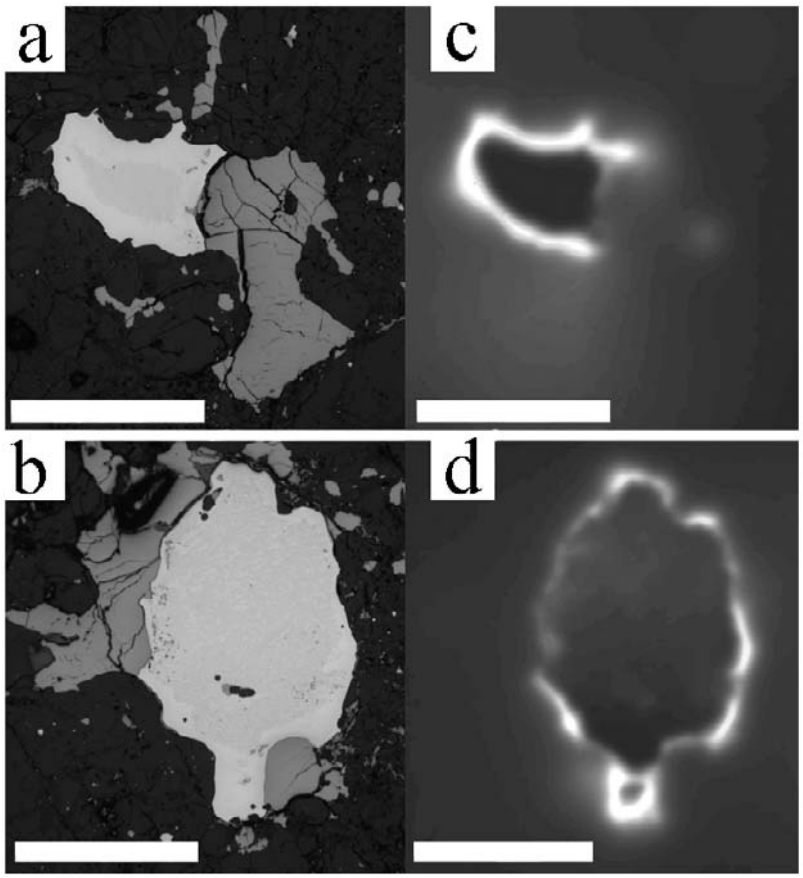

Figure 4. (a and b) Reflected light and (c and d) direct MO images of metallic FeNi grains (bright in the reflected light images) in a polished thick section of the Ausson (L5) chondrite meteorite showing imperfect surrounding rims in the direct MO images. The sample carries an out-of-page pointing SIRM (demagnetized at 10 mT AF). Darker gray nonmagnetic grains in the optical images are troilite. Figures 4a and 4c depict a grain showing a broken rim MO pattern. Figures 4b and 4d depict a grain showing an intermittent rim MO pattern. The thickness of the thinnest portion of the rim is 10 μm. Scale bars are 300 μm.

component over the grain would result in perpendicular flux at the edges due to flux closure, and could account for the rimmed MO pattern. However, the closed flux configuration would imply a magnetic singularity at the grain center. Such a singularity as in a magnetic vortex or very strong downward magnetic field is not observed. We can therefore safely exclude this third hypothesis.

[15] The results exemplify the high spatial resolution of the MOI technique. A close-up image (Figures 4b and 4d) demonstrates that the MOI technique can be used to visualize a 10 μm magnetic structure. Such high spatial resolution is due to the small thickness of the MO active layer (5 μm) and the small sample-to-indicator distance, which allow us to measure only the near-field contributions of the sample's stray fields. Since the magnetic field decays quadratically with distance in this configuration, this small sample-to-indicator distance compensates for the low sensitivity of the indicator. *Bobyl et al.* [2007] showed that the actual sample-to-indicator distance can be measured by observing a small gap (<10 μm) between two magnetic grains separated by a nonmagnetic material. In the experiment of *Bobyl et al.* [2007], this distance was 2.5 μm. Although we did not experimentally estimate the sample-to-indicator distance in the present study due to the large intergrain distance within the observed samples (Figure 3), this distance is probably the same as in the previous study in view of the similar material and experimental setup.

[16] Figure 5 shows direct MO images at different sample-to-indicator distances for solid and rim-like MO patterns. Figure 5a demonstrates that the contrast of solid MO patterns is progressively

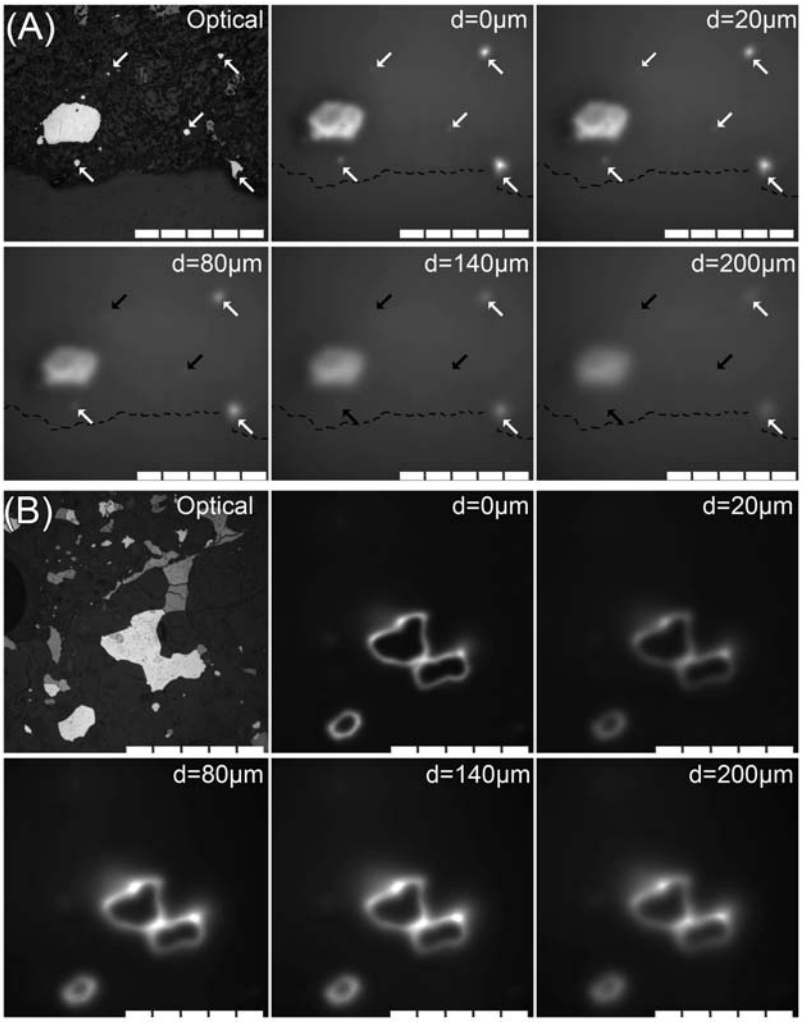

Figure 5. Direct MO images of metal grains in meteorites at different sample-to-indicator distances adjusted by use of 20 μm thick plastic films. The samples carry an out-of-page pointing SIRM demagnetized at 10 mT AF. Bright grains in the reflected light microscopic images ("optical") are Fe-Ni grains, and darker grains are troilite. The silicate matrix is dark. (a) Polished thin section of Borgo San Donino (H5) ordinary chondrite meteorite. The largest metal grain shows magnetic inner texture without rim. Smaller grains also show magnetic signals (white arrows), but the signals are diminished at large distances (black arrows). (b) Polished thick section of Agen (H5) ordinary chondrite meteorite (see also Figure 3). MO image shows clear rim structure. Scale bars are 500 μm.

diminished and the image is more and more diffuse, with loss of the detailed features as one increases the distance between sample and indicator. Finally, small magnetized regions completely vanish from the image. It is interesting to note that the rim-like MO patterns keep their ring feature even for large indicator-to-sample distances (Figure 5b). In the image covering the whole sample (Figure 3), one observes only diffuse solid MO patterns and no diffuse rim-like MO patterns. This suggests that rim-like MO patterns appear only on a cut surface of the zoned Fe-Ni grain.

[17] The quantification of magneto-optical images can be conducted through ad hoc calibration procedure. Equations (1) and (4) have that the intensity of the MOI image is

$$I_{MOI} \approx 4\,d\;V\,M_s I_0 \left(T_{\parallel} - T_{\perp}\right)\theta \arctan\left[B_{\perp}/\left(B_{\parallel} + B_{\mathrm{k}}\right)\right] + I_0\,T_{\perp}. \tag{6}$$

From equations (1) and (5), the differential MOI image can be written as

$$\Delta I_{MOI} \approx 4\,d\;V\,M_s\,I_0\,T_{\parallel}\Delta\theta \arctan\left[B_{\perp}/\left(B_{\parallel} + B_{\mathrm{k}}\right)\right]. \tag{7}$$

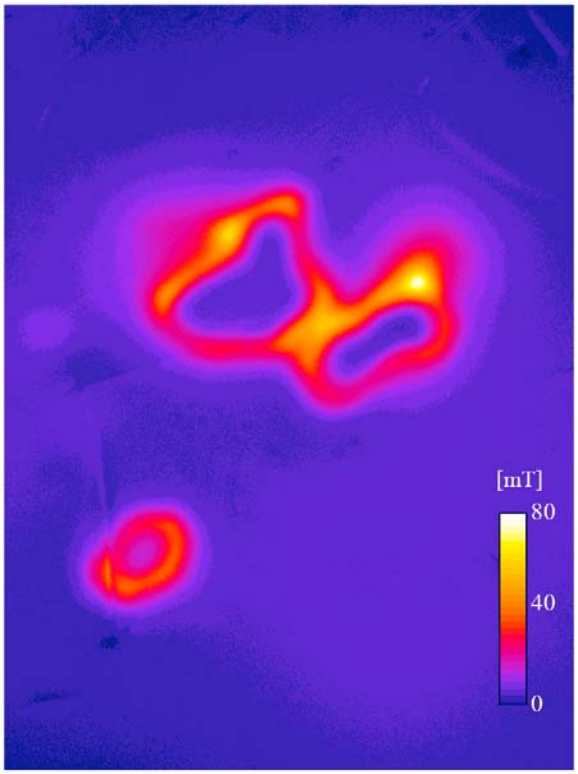

Figure 6. Calibrated MOI image of metallic grains in Agen (H5) meteorite. The observed region is same as that used in Figure 5b. The scale indicates the absolute field value. The direction of the field is generally upward except for the interior of the ring-shaped rim structure. The peak value (whitish color) is underestimated due to the saturation of the indicator.

The analyzer angle θ and the difference of the angle $\Delta\theta$ are measurable. We have already measured the characteristics of the indicator, such ($2\ d\ V\ M_s$) = 0.122° and B_k = 32.8 mT. Although these values are not homogeneous over the indicator, we can reduce the error by averaging several images acquired with different spatial positions of the indicator. Thus, using these values and assuming a given intensity of the illumination, one can estimate $B_\perp$ using equation (6) or (7).

[18] However, there is additional source of uncertainty in the presence of in-plane magnetic fields. Indeed, according to equation (1), the in-plane component ($B_\parallel$) will result in an underestimation of α_F. Although this results in negligible (<1%) error for weak magnetic fields ($B_\parallel \ll B_k$), such as stray fields from samples carrying a NRM, this may lead to significant underestimation in case of sample carrying a saturation remanent magnetization. If we consider a thin section (30 μm thick) with a magnetite or FeNi grain of lateral dimensions 300 μm, carrying a homogeneous vertical SIRM (about 1×10^5 Am^{-1} for both typical magnetite and FeNi), we can compute through forward modeling [e.g., *Quesnel et al.*, 2008] that a maximum in-plane field $B_\parallel$ = 20 mT will thread an indicator situated 3 μm above the sample plane. This will result in an underestimation of $B_\perp$ of 50% at the edge of the grain, but will not induce any error at the grain center where $B_\parallel$ = 0 mT. A straightforward calculation of $B_\parallel$ can then remove the underestimation at the edge. Furthermore, spatial variations of the illumination I_0, which cannot be cancelled by taking the mean of several images, should also be accounted for whilst calibrating. However, the modulation technique vastly reduces this source of error.

[19] Figure 6 shows a quantitative image of the perpendicular field distribution around the metal grain observed in Figure 5b. The calibration was performed by increasing a perpendicular magnetic field from 0 to 55 mT in 1 mT steps, without removing the indicator from the sample, and taking an image at each step. The field strength is calibrated with a Hall probe at the sample location before the imaging. The image intensity in a selected portion of the image, in proximity to the grain but avoiding any soft magnetic inclusions, is then fitted against field strength. This is tantamount to determining the parameters in equation (6). Finally, image intensities are converted to local values of $B_\perp$. Since the maximum field intensity (~80 mT) in the image is very high, the MOI image was taken at θ = 0° to avoid saturation of the CCD camera; hence, the scale shows the absolute value of $B_\perp$. This procedure demonstrates that MOI images can be accurately converted into a map of the perpendicular magnetic induction through a calibration procedure. The presented method is very robust because the calibration and the measurement are simultaneously conducted, but has the drawback that the sample was subjected to a magnetic field. The utilized magnitude of the field does not alter the saturation magnetization, but may alter a natural remanent magnetization. Although this will affect accuracy, this can be resolved by making separate calibration and measurement runs. Finally, we present differential MO images (ΔI_{MOI}) of a sample (Ensisheim LL6 ordinary chondrite) with its original NRM (Figure 7). Owing to their high signal-to-noise ratio, the differential images obtained by the modulation technique show clear magnetic patterns. The magnetic image shows that

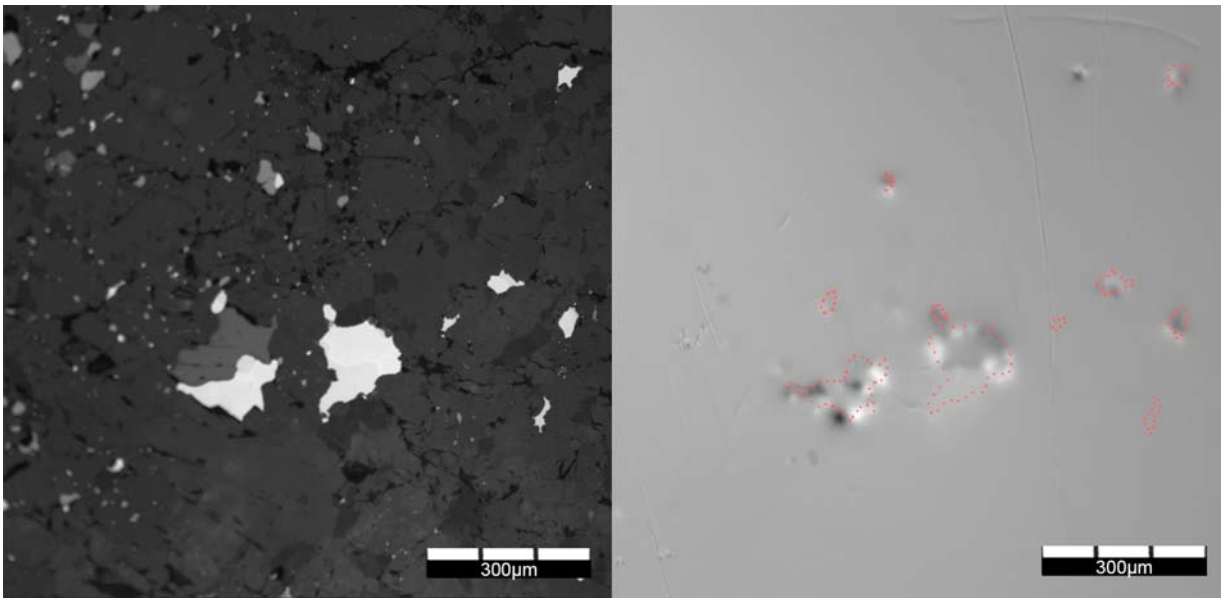

Figure 7. (left) Reflected light microscopic image and (right) differential MO image showing a polished thick section of Ensisheim LL6 meteorite carrying its natural remanent magnetization. Metallic grains (bright in optical image) show small-scale (<100 μm) magnetic dipole-like feature. The larger two grains show several dipole-like features within a grain, whereas the other smaller grains tend to show single dipole feature within a grain. Dotted lines in the magnetic image indicate outlines of metal grains. Scale bars are 300 μm.

the metallic grains in the meteorite carry an NRM, and that the declinations of the NRM vectors of individual grains, which can be roughly estimated by the dipole-like features, are not homogeneously oriented as was already observed in LL6 ordinary chondrites by bulk measurements on the mm scale [e.g., *Morden and Collinson*, 1992; *Gattacceca et al.*, 2003]. Moreover, single large metallic grains contain multiple dipole-like features with typical scale of several dozen micrometers. The directions of these magnetic signatures are not uniform. It suggests that the NRM is not homogeneously oriented even within single metallic grains.

4. Conclusions

[20] We have adapted a magneto-optical imaging system to the observation of polished rock samples. This system images the vertical component of the magnetic field above the samples, thus allowing for mapping of the remanence carriers in rocks. Quantification of the magnetic field can be achieved through a calibration procedure that is, however, specific to given experimental settings (temperature, light intensity, modulation angle, etc). This technique can map stray fields from both artificial and natural magnetizations of polished rock samples with a spatial resolution of the order of 10 μm. Weakly magnetized samples can be studied through the use of a polarization modulation technique. One of the main advantages of this magneto-optical system is that it allows direct comparison of the magnetic images with reflected light images, a crucial advantage to identify remanence carriers in rocks.

Acknowledgments

[21] M.U. was funded by a Research Fellowship of the Japan Society for the Promotion of Science for Young Scientists and by the Institut des Sciences de l'Univers. We thank B. Zanda (MNHN, France) for the meteorite samples. This work was funded by the Agence Nationale de la Recherche (project ANR-05-JCJC-0133). This paper benefited from constructive reviews by B. M. Moskowitz and two anonymous reviewers.

References

Bending, S. J., et al. (2004), Comparison of magneto-optical imaging with other local magnetic probes, in *Magneto-Optical Imaging*, edited by T. H. Johansen and D. V. Shantsev, pp. 11–18, Kluwer Acad., Dordrecht, Netherlands.

Bobyl, A. V., Y. Y. Podladchikov, H. Austrheim, B. Jamtveit, T. H. Johansen, and D. V. Shantsev (2007), Magnetic field visualization of magnetic minerals and grain boundary regions using magneto-optical imaging, *J. Geophys. Res.*, *112*, B04105, doi:10.1029/2006JB004305.

Dorosinskii, L. A., et al. (1992), Studies of HTSC crystal magnetization features using indicator magnetooptic films with in-plane anisotropy, *Physica C*, *203*(1–2), 149–156.

Flament, S., et al. (2004), Magneto optical imaging of vortex penetration in patterned YBCO thin film near Tc, in *Magneto-Optical Imaging*, edited by T. H. Johansen and D. V. Shantsev, pp. 191–196, Kluwer Acad., Dordrecht, Netherlands.

Gattacceca, J., et al. (2003), Magnetic properties of a freshly fallen LL ordinary chondrite: The Bensour meteorite, *Physics Earth Planet. Inter.*, *140*(4), 343–358.

Gattacceca, J., et al. (2006), Investigating impact demagnetization through laser impacts and SQUID microscopy, *Geology*, *34*(5), 333–336.

Hankard, F., J. Gattacceca, C. Fermon, M. Pannetier-Lecoeur, B. Langlais, Y. Quesnel, P. Rochette, and S. A. McEnroe (2009), Magnetic field microscopy of rock samples using a giant magnetoresistance-based scanning magnetometer, *Geochem. Geophys. Geosyst.*, *10*, Q10Y06, doi:10.1029/2009GC002750.

Hoffmann, V., et al. (1990), Quantitative magneto-optical Kerr effect on titanomagnetites, *Phys. Earth Planet. Inter.*, *65*(1–2), 28–35.

Indenbom, M. V., et al. (2002), Visualization of magnetic structures in superconductors and magnetic materials using magneto-optical garnet films, *J. Magn. Soc. Jpn.*, *26*(10), 244–247.

Jooss, C., et al. (2002), Magneto-optical studies of current distributions in high-Tc superconductors, *Rep. Prog. Phys.*, *65* (5), 651–788.

Morden, S. J., and D. W. Collinson (1992), The implications of the magnetism of ordinary chondrite meteorites, *Earth Planet. Sci. Lett.*, *109*(1), 185–204.

Nagata, T., and M. Funaki (1982), Magnetic properties of tetrataenite-rich stony meteorites, *Mem. Natl. Inst. Polar Res.*, *25*, 222–250.

Nagata, T., et al. (1986), Magnetic properties of tetrataenite-rich meteorites II, *Mem. Natl. Inst. Polar Res.*, *41*, 364–381.

Polyanski, A. A., et al. (1999), Visualisation of magnetic flux in magnetic materials and high temperature superconductors using the Faraday effect in ferrimagnetic garnet films, in *Nano-Crystalline and Thin Film Magnetic Oxides*, edited by I. Nedkov and M. Ausloos, pp. 353–369, Kluwer Acad., Dordrecht, Netherlands.

Polyanskii, A., et al. (2004), Magneto-optical investigation of superconducting materials, in *Magneto-Optical Imaging*, edited by T. H. Johansen and D. V. Shantsev, pp. 19–28, Kluwer Acad., Dordrecht, Netherlands.

Quesnel, Y., et al. (2008), Modelling and inversion of local magnetic anomalies, *J. Geophys. Eng.*, *5*, 387–400.

Reisener, R. J., and J. I. Goldstein (2003), Ordinary chondrite metallography: Part 2. Formation of zoned and unzoned metal particles in relatively unshocked H, L, and LL chondrites, *Meteorit. Planet. Sci.*, *38*(11), 1679–1696.

Uehara, M., and N. Nakamura (2008), Identification of stable remanence carriers through a magneto-impedance scanning magnetic microscope, *Stud. Geophys. Geod.*, *52*(2), 211–223.

Weiss, B. P., E. A. Lima, L. E. Fong, and F. J. Baudenbacher (2007), Paleomagnetic analysis using SQUID microscopy, *J. Geophys. Res.*, *112*, B09105, doi:10.1029/2007JB004940.

Welp, U., et al. (2003), Magnetic domain structure and magnetic anisotropy in $Ga_{1-x}Mn_xAs$, *Phys. Rev. Lett.*, *90*, 167206.